Earth and Planetary Science Letters 413 (2015) 1–12

Contents lists available at ScienceDirect

Earth and Planetary Science Letters

www.elsevier.com/locate/epsl

Megacrystals track magma convection between reservoir and surface

Yves Moussallam [a,b,*], Clive Oppenheimer [a], Bruno Scaillet [b], Iris Buisman [c], Christine Kimball [d], Nelia Dunbar [e], Alain Burgisser [f,g], C. Ian Schipper [b,h], Joan Andújar [b], Philip Kyle [d]

[a] Department of Geography, University of Cambridge, Downing Place, Cambridge, CB2 3EN, UK
[b] ISTO, 7327 Université d'Orléans-CNRS-BRGM, 1A rue de la Férollerie, 45071 Orléans cedex 2, France
[c] Department of Earth Sciences, University of Cambridge, Downing Street, Cambridge, CB2 3EQ, UK
[d] Department of Earth and Environmental Science, New Mexico Institute of Mining and Technology, 801 Leroy Place, Socorro, NM 87801, USA
[e] New Mexico Bureau of Geology and Mineral Resources, New Mexico Institute of Mining and Technology, 801 Leroy Place, Socorro, NM 87801, USA
[f] CNRS, ISTerre, F-73376 Le Bourget du Lac, France
[g] Université de Savoie, ISTerre, F-73376 Le Bourget du Lac, France
[h] School of Geography, Environment and Earth Sciences, Victoria University, PO Box 600, Wellington, New Zealand

ARTICLE INFO

Article history:
Received 1 April 2014
Received in revised form 9 December 2014
Accepted 11 December 2014
Available online 13 January 2015
Editor: T. Elliott

Keywords:
convection
bi-directional flow
megacrystal
anorthoclase
crystal zoning
melt inclusion

ABSTRACT

Active volcanoes are typically fed by magmatic reservoirs situated within the upper crust. The development of thermal and/or compositional gradients in such magma chambers may lead to vigorous convection as inferred from theoretical models and evidence for magma mixing recorded in volcanic rocks. Bi-directional flow is also inferred to prevail in the conduits of numerous persistently-active volcanoes based on observed gas and thermal emissions at the surface, as well as experiments with analogue models. However, more direct evidence for such exchange flows has hitherto been lacking. Here, we analyse the remarkable oscillatory zoning of anorthoclase feldspar megacrystals erupted from the lava lake of Erebus volcano, Antarctica. A comprehensive approach, combining phase equilibria, solubility experiments and melt inclusion and textural analyses shows that the chemical profiles are best explained as a result of multiple episodes of magma transport between a deeper reservoir and the lava lake at the surface. Individual crystals have repeatedly travelled up-and-down the plumbing system, over distances of up to several kilometers, presumably as a consequence of entrainment in the bulk magma flow. Our findings thus corroborate the model of bi-directional flow in magmatic conduits. They also imply contrasting flow regimes in reservoir and conduit, with vigorous convection in the former (regular convective cycles of ~150 days at a speed of ~0.5 mm s^{-1}) and more complex cycles of exchange flow and re-entrainment in the latter. We estimate that typical, 1-cm-wide crystals should be at least 14 years old, and can record several (from 1 to 3) complete cycles between the reservoir and the lava lake via the conduit. This persistent recycling of phonolitic magma is likely sustained by CO_2 fluxing, suggesting that accumulation of mafic magma in the lower crust is volumetrically more significant than that of evolved magma within the edifice.

1. Introduction

Many volcanoes, such as Etna and Stromboli in Italy, persistently emit prodigious quantities of gas and heat at the surface without significant accompanying lava flows or tephra production (Francis et al., 1993). The decoupling of gas and thermal energy from the magma efflux has been investigated in several theoretical and experimental treatments that consider exchange flow between two fluids of contrasting density and viscosity (Kazahaya et al., 1994; Stevenson and Blake, 1998; Huppert and Hallworth, 2007; Beckett et al., 2011). These studies suggest that a stable bi-directional flow can develop in volcanic conduits, and reinforce interpretations of the magma dynamics of a number of persistently degassing volcanoes (e.g., Oppenheimer et al., 2009; Shinohara and Tanaka, 2012). Conduit convection suggests substantial endogenous growth of volcanoes (Francis et al., 1993; Allard, 1997) and may explain melt inclusion trends associated with degassing volcanoes (Witham, 2011). While the conclusion that magma convects in conduits feeding many open vent volcanoes seems inescapable, direct evidence has been lacking.

* Corresponding author at: ISTO, 7327 Université d'Orléans-CNRS-BRGM, 1A rue de la Férollerie, 45071 Orléans cedex 2, France.
E-mail address: yves.moussallam@cnrs-orleans.fr (Y. Moussallam).

http://dx.doi.org/10.1016/j.epsl.2014.12.022

The potential of zoned crystals to record chemical and physical changes experienced by their host magma has long been recognised (see review by Ginibre et al., 2007). Oscillatory zoning in feldspar is a common phenomenon with several inferred origins. Two main schools of thought have prevailed, originating from studies in the 1920s, and broadly evoke either extrinsic (Bowen, 1928) or intrinsic (Harloff, 1927) mechanisms. The extrinsic school argues that zonation reflects changing pressure, temperature, composition and volatile content of the melt surrounding the crystal via processes such as convection (e.g., Singer et al., 1995) and episodic fluctuations in magma supply. The intrinsic school points to the widely-observed lack of correlation of oscillatory layers between crystals (e.g., Wiebe, 1968; Shore and Fowler, 1996) and argues instead that kinetic processes at the crystal-melt interface are responsible for zonation (e.g., Allegre et al., 1981; L'Heureux and Fowler, 1996). The kinetic models imply high degrees of undercooling at the boundary layer and reproduce the typical sawtooth patterns revealed in electron microprobe (EMP) traverses of oscillatory-zoned feldspar crystals. However, these intrinsic models cannot reproduce low amplitude variations. Nor do they explain multiple resorption episodes, evident in many oscillatory-zoned crystals. Recent studies have highlighted how both mechanisms for generating oscillatory zoning can be manifested in single crystals (e.g. Viccaro et al., 2010), and have used mineral compositional zoning to identify a variety of magmatic processes such as magma recharge, mixing and degassing (e.g., Humphreys et al., 2006; Charlier et al., 2008; Kahl et al., 2013).

Erebus volcano (Antarctica) is renowned for its long-lived phonolitic lava lake, whose behaviour has been explained in terms of the conduit exchange-flow model (Oppenheimer et al., 2009). It is also remarkable for the impressive size to which its most abundant mineral phase, anorthoclase feldspar, grows (Kyle, 1977; Dunbar et al., 1994). These anorthoclase megacrystals (up to 10-cm-long) display exceptional oscillatory zoning and large (up to 600-μm-diameter) melt inclusions (Fig. 1). In this study, we analyse the major element composition of natural anorthoclase crystals and major element and volatile compositions of enclosed melt inclusions, and compare them to anorthoclase crystals and associated melts derived by phase equilibrium and solubility experiments. The experimental data provide a tightly-constrained framework with which to interpret the natural zoning and to retrace the growth history of individual anorthoclase megacrystals.

We start with a brief overview of the Erebus phonolite phase assemblage, including a description of the natural anorthoclase megacrystals, and then describe the different experimental and analytical methods used in this study. We present the results of phase equilibrium experiments, and compare the chemistry of synthetic and natural anorthoclase. We then describe solubility experiments and their relation to analyses of melt inclusions and their host zone within natural crystals. Lastly, we link the chemical zoning in natural anorthoclase to the timescales of magma ascent and descent.

2. Background information

2.1. Mineral assemblage

Erebus volcano (3794 m, 77.58°S, 161.17°E), hosts the world's only phonolitic lava lake. This lava lake appears to have been persistently degassing since the volcano was first observed by James Ross in 1841. This current passive activity is sporadically interrupted by Strombolian explosions that eject fresh bombs on to the crater rim. All bombs analysed since 1972 are virtually identical in terms of mineral assemblage (with one exception) and whole rock and matrix glass major, minor and trace elements (Kelly et al., 2008). This chemical stability extends to older lava flows, such that all lavas erupted from Erebus in the last 20 ka have the same composition (Kelly et al., 2008) making the volcano an ideal system to investigate using experimental petrology tools at equilibrium conditions.

Phonolite bombs are composed chiefly of vesicular matrix glass (~67 vol%; fragile, easily disintegrated and microlite-free) and anorthoclase feldspar (~30 vol%) with minor amounts of titanomagnetite (~1.1 vol%), olivine (~0.8 vol%), clinopyroxene (~0.6 vol%) and fluorapatite (~0.5 vol%), and lesser quantities of pyrrhotite blebs (Kyle et al., 1992; Kelly et al., 2008). Of all mineral phases (described in detailed by Kelly et al., 2008) anorthoclase is the only mineral with compositional zoning.

2.2. Anorthoclase megacrystals

Euhedral anorthoclase feldspar in phonolite bombs are zoned with respect to major (Fig. 1) and trace (Sumner, 2007) elements. The compositional zoning occurs at a variety of scales: the lowest frequency variations shown by some crystals (Fig. 2) have wavelengths of ~5 mm and amplitude of ~7 mol% (Or) while higher-frequency variations have a typical wavelength of $\lesssim$800 μm and amplitude of $\lesssim$4 $mol\%_{Or}$. Inter-zone variations are in the range of Ab_{61-66}, An_{21-10}, and Or_{14-28} (with Ab, An and Or referring to the albite, anorthite and orthoclase end members respectively; Fig. 2). Small-scale elemental maps (Fig. 1) reveal embayment at some zone boundaries, indicating resorption episodes. Hosted in the anorthoclase crystals are large (usually <600 μm across) phonolitic melt inclusions, typically trapped in single growth layers of the anorthoclase (Fig. 1). Natural anorthoclase megacrystals presented in this study were manually separated from phonolitic bombs erupted in 1984 and 2005 (Fig. S1; Table S1).

3. Methods

3.1. Phase equilibria and solubility experiments

The starting material (ERE 97018) used in all experiments is a phonolitic bomb erupted in 1997 and collected at the crater rim (described in Moussallam et al., 2013). All phase equilibria experiments are described in Moussallam et al. (2013) and the present study uses a subset of those experiments whose conditions closely reproduced the natural mineral assemblage.

Water- and CO_2-solubility experiments were conducted across a range of pressures (50, 100, 200, and 300 MPa), temperatures (950 and 1000 °C), and X_{H_2O} (mole fraction of water in the fluid phase, from near 0 to 1) under reduced conditions ($fO_2 \approx$ QFM or below; with QFM being the quartz–fayalite–magnetite redox buffer). We used internally-heated pressure vessels at the ISTO laboratory in Orléans, which can reach pressures of up to 400 MPa under controlled temperatures (up to 1200 °C) and oxygen fugacity conditions. The vessel was pressurised using an argon–hydrogen gas mixture as the pressure medium to control redox state (Scaillet et al., 1992). Heating was applied by a double-wound molybdenum furnace creating a stable "hot-spot" zone. Two S-type thermocouples located on either side of this 5-cm-long "hot-spot" permitted precise control of the heating resistances thus preventing the establishment of thermal gradients.

Experimental charges consisted of natural anhydrous sample powder (30 mg) with $X_{H_2O,loaded}$ [= mole fraction of H_2O added to the capsule, $H_2O/(H_2O+CO_2)$] varying from 0 to 1 (i.e. pure CO_2 to pure H_2O) and loaded in gold capsules (2 cm in length, with 2.5 mm inner diameter and 2.9 mm outer diameter). The capsules were wrapped in liquid nitrogen-soaked tissue to prevent water loss and welded shut. For each experiment, six capsules were placed in a sample holder hung by a thin Pt wire. The temperature gradient along the "hot-spot" zone where the capsules were located was always <2 °C. Rapid quenching was assured by

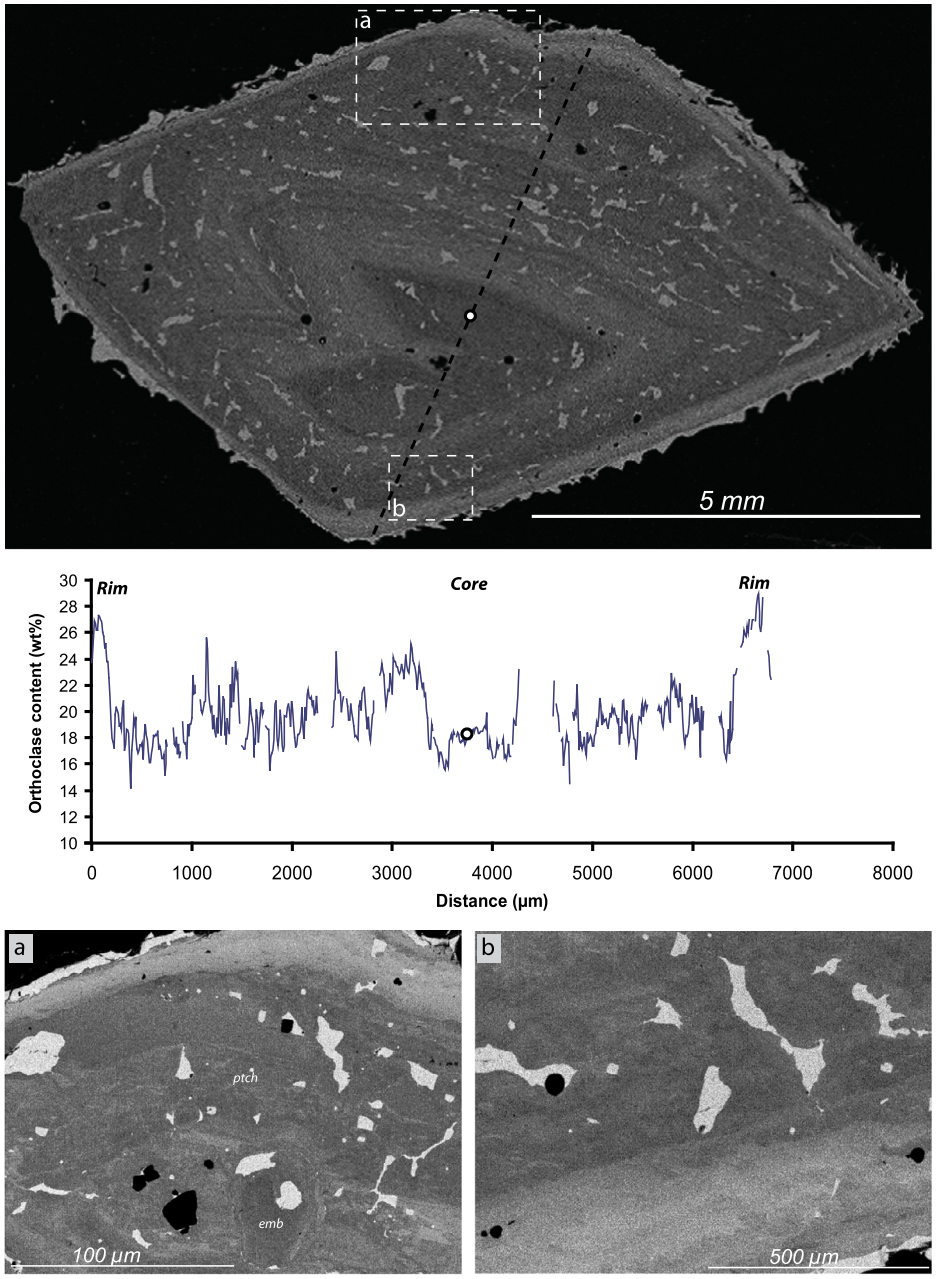

Fig. 1. Upper panel: Potassium X-ray maps of a sectioned anorthoclase crystal (sample *eb*05027*a*2) showing remarkable oscillatory zoning. Irregularly-shaped melt inclusions are clearly visible as brighter (K-rich) areas. Central panel: EMP transect reported in terms of orthoclase end member content (in %). The location of the transect in shown on the X-ray map; the white circles show corresponding points between the analysis and the crystal. The starting point of the transect is the upper right portion of the crystal. Gaps in the transect indicate the presence of melt inclusions. Lower panel: left hand side: Close-up potassium X-ray maps of area (a), the location of which is shown on upper panel map. Notice the patchiness of the central zones (labelled *ptch*) and the embayed zone boundaries (labelled *emb*), both textures indicative of out of equilibrium, resorption events. Right hand side: Close-up potassium X-ray maps of area (b), the location of which is shown on upper panel map. This map shows the strong contrast between the last two zones closest to the rim of the crystal, the relatively straight boundary and gradual change of composition.

passing an electrical current to the holding Pt wire (Di Carlo et al., 2006), such that the sample dropped into the cold part of the vessel, providing a cooling rate of $>100\,^{\circ}\mathrm{C\,s^{-1}}$. After each experiment, capsules were weighed to verify that no leakage had occurred. They were then opened and part of the charge (as a single fragment) was embedded in an epoxy resin and polished for SEM, secondary ion mass spectrometry (SIMS) and electron microprobe analyses (see Section 3.3 below).

3.2. Micro-tomography

X-ray micro-tomography (μ-CT) analyses of individual anorthoclase crystals were performed with a Phoenix Nanotom 180 at ISTO in Orléans in order to confirm whether or not the melt inclusions they hosted were isolated from each other. We used a molybdenum target, tungsten filament, operating voltage of 100 kV, filament current of 80 μA, and 2 s exposure time. Whole crystals (from 1 to 5 cm in length) were mounted on to carbon fibre rods using Araldite epoxy resin. The samples were rotated through 360° during exposure. About 2300 images were collected during each analysis, each of them being an average of four raw images taken at 2 s intervals. Reconstruction of these images into a stack of greyscale images representing different phases was performed with a PC micro-cluster running commercial software. The voxel edge length for most scans was 6–11 μm. This was sufficient to

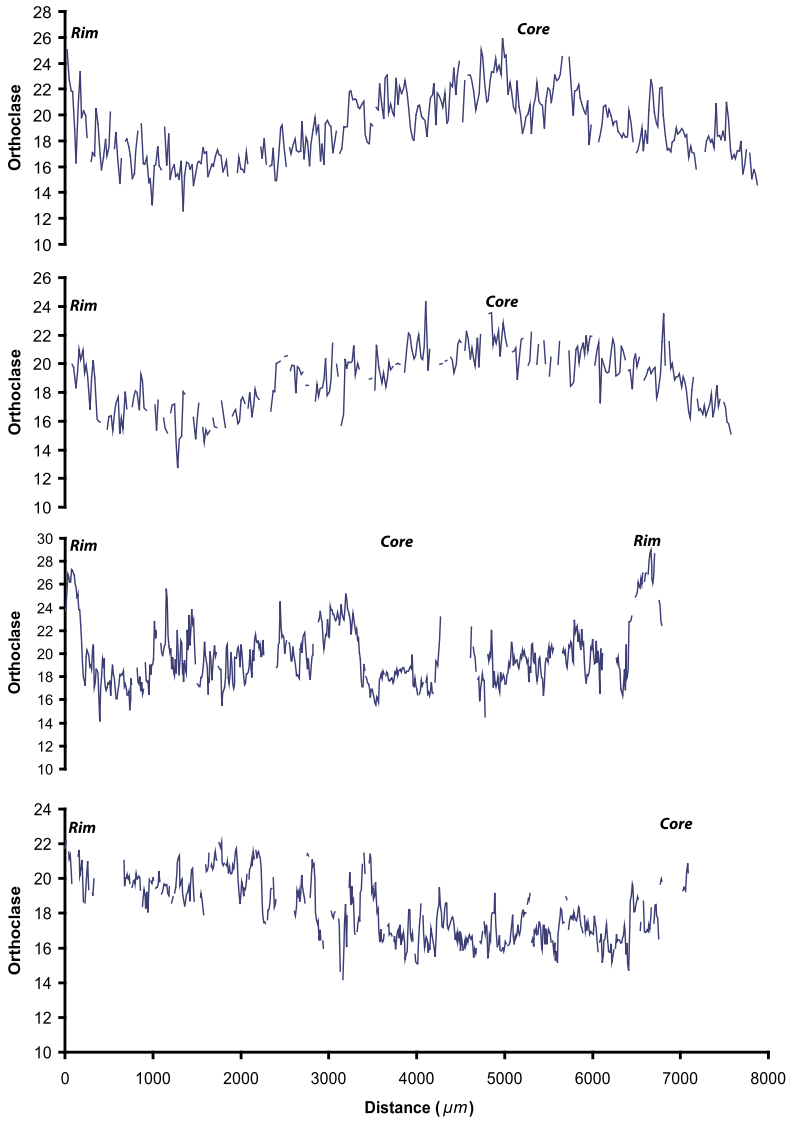

Fig. 2. EMP transect reported in terms of orthoclase content (in %) for crystals (from top to bottom): Ere_1984_03_S2, Ere_1984_XC_06_S2, eb05027a2 and eb05042b2. Gaps are due to melt inclusions.

resolve the geometry of most melt inclusions; however, inclusions smaller than 11 μm could not be imaged.

Image processing was handled using the ImageJ freeware (http://rsbweb.nih.gov/ij/). Original images were converted to 8 bits and a median filter was applied to reduce noise. Image contrast was enhanced using a fuzzy contrast enhancement algorithm tuned to highlight the inclusions. Images were then converted to binary; outlier pixels were removed; and a second median filter was applied. This thresholded image set was combined with another set of images thresholded so as to characterise the melt outside the crystal. This enabled a particle analyser algorithm to identify any melt inclusions that were connected with the glass surrounding the crystal. The algorithm was also used to identify any interconnected inclusions. Final image sets were handled using the VGStudio MAX software to obtain 3D image representations.

3.3. Analytical techniques (SIMS and EMPA)

Electron microprobe analyses of synthetic anorthoclase crystals, and natural melt inclusions and their host crystal zones were performed on a Cameca SX-100 at the Department of Earth Sciences, University of Cambridge, and on a Cameca SX-100 at New Mexico Institute of Mining and Technology. Rim-to-rim and core-to-rim profiles were acquired at 10 μm step spacing along 7000–8000 μm distances. For glass analyses, we used an accelerating voltage of 15 kV, a beam current of 2 nA and a defocused beam of 10 μm to measure Si, Ti, Al, Fe, Mn, Mg, Ca, Na and K. For synthetic mineral phases, the same elements were analysed with an accelerating voltage of 10 kV, a beam current of 6 nA and a focused beam at 1 μm. X-ray maps were acquired using a 100 nA beam current and 15 kV accelerating voltage with a 10–13 μm step size and 12 ms dwell time. Na and K were analysed first in order to minimise alkali loss during analysis.

SIMS analyses of volatiles (CO_2 and H_2O) in natural melt inclusions and synthetic melts produced by solubility experiments were performed on a Cameca ims-4f and a Cameca ims-1280 at the NERC Ion Microprobe Facility at the University of Edinburgh. On the Cameca ims-4f, measurements were made using a primary O^- ion beam with an accelerating voltage of 15 kV and a beam current of 5 nA, a secondary accelerating voltage of 4500 V minus a 50 V offset, and a 25 μm image field. On the Cameca ims-1280, measurements were made using a primary O^- ion beam with an accelerating voltage of 10 kV and a beam current of 5 nA. On both instruments, the ion beam was rastered over an area of ap-

proximately 40 μm^2 for >60 s prior to analysis to remove surface contamination. A 10 μm × 10 μm beam, centred in the middle of the rastered area was then used for measurements. The following isotopes were measured for 15 cycles on the ims-4f, with counting times in seconds in parentheses: $^{1}H^{+}$ (5), $^{24}Mg^{2+}$ (5), ^{12}C (10), ^{17}O (2) and ^{30}Si (2). Only counts from the final 10 cycles, when count rates reach an asymptote and the effects of surface contamination are minimal, were retained to calculate O and C concentrations. On the ims-1280, the following isotopes were measured for 10 cycles with counting times in seconds in parentheses: $^{1}H^{+}$ (5), $^{24}Mg^{2+}$ (2), ^{12}C (6), ^{16}O (2), ^{17}O (4), ^{19}F (6), ^{30}Si (2), ^{32}S (6), ^{35}Cl (6). Precision at 1σ was estimated as 10% using repeat analyses of samples.

4. Results

4.1. Comparing synthetic and natural feldspar compositions

We analysed the composition of synthetic anorthoclase produced in crystallisation experiments by Moussallam et al. (2013) (see Methods therein) over pressure and temperature ranges of 0.1–100 MPa and 900–1000 °C, respectively, with varying fluid composition. The original experiments constrained the stability field of the Erebus phonolite assemblage (i.e. the conditions within which the natural erupting assemblage is experimentally reproduced) to pressures less than 200 MPa, temperature of 950 ± 25 °C, H_2O content less than 0.2 wt% and fO_2 of QFM to QFM-1.

The bulk composition of the natural anorthoclase is $Ab_{65.8}$, $An_{16.2}$, $Or_{17.9}$. Inter-zone variations are in the range of $Ab_{61–66}$, $An_{21–10}$, and $Or_{14–28}$ (Fig. 2). The effects of pressure and temperature on the composition of the crystallising synthetic anorthoclase are shown in Fig. 3 (see also Table S2). While chemical variations cannot be linked confidently to the modal abundance (or composition) of a single phase, temperature variations alone cannot account for the range of compositions observed in the natural anorthoclase feldspar at a fixed growth pressure. The possible temperature range of the natural system is narrow and well established: it cannot be colder than 925 °C or biotite, a phase never observed in Erebus lavas, would crystallise. Conversely, it cannot be hotter than 975 °C because the observed anorthoclase crystals would resorb. This narrow range limits the possible feldspar composition such that not all observed compositions can be achieved at a given pressure. If, for instance, all feldspar growth were taking place in the lava lake, the lowest Or and highest An contents in the natural feldspar could not be reproduced.

As with temperature, variations in water content cannot play a significant role in generating the compositional diversity, since Erebus phonolite has very low water abundance (H_2O < 0.2 wt%; see also Section 4.2). In contrast, pressure variations alone are seemingly able to reproduce the range in composition observed in natural feldspar (extrapolating to pressures greater than 100 MPa), suggesting that the observed oscillatory zoning must, at least partly, reflect crystal growth at different depths in the magma plumbing system. As we show below, analyses of melt volatile contents provide another line of evidence that changes in pressure rather than in temperature are dominant in the Erebus magmatic system.

4.2. Comparing synthetic and natural volatile melt contents

In order to relate the melt inclusion volatile contents to their entrapment depth, we performed a series of CO_2–H_2O solubility experiments on the Erebus phonolite composition (Fig. 4). This set of experiments describes the solubility behaviour of CO_2–H_2O species in the fluid-saturated Erebus phonolite melt. Given that the natural phonolite H_2O content in glass and MI is lower than

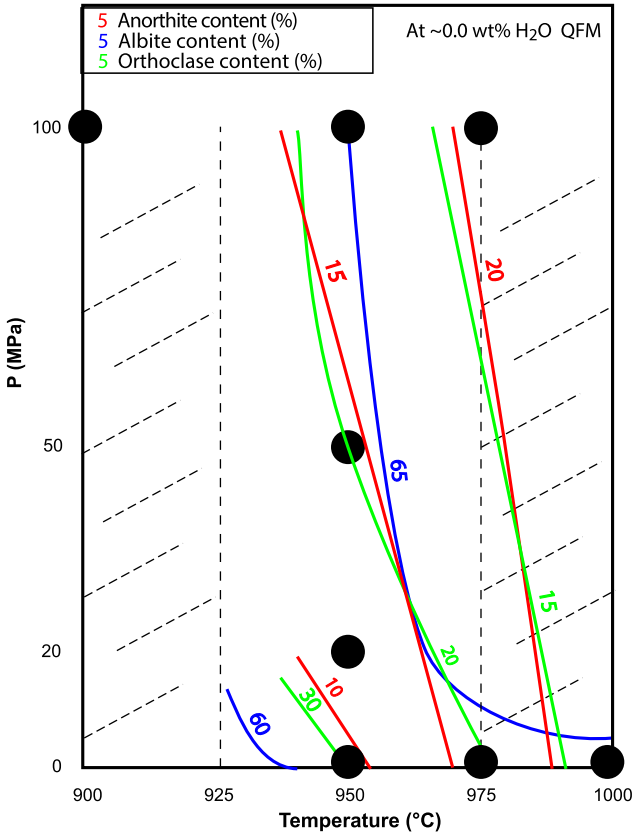

Fig. 3. Temperature *vs.* pressure plot showing anorthoclase composition in terms of end members within Erebus phonolite under dry conditions and log(fO_2) near QFM to QFM-1. Filled black circles represent P–T conditions of individual experimental charges. Dashed areas represent conditions outside the stability field of the Erebus phonolitic assemblage. The blue, red and green lines represent albite, anorthite and orthoclase isopleths, with labels in regular, bold and italic font respectively. The numerical values of the labels cover the range of natural composition ($Ab_{61–66}$, $An_{21–10}$, $Or_{14–28}$). (For interpretation of the references to colour in this figure legend, the reader is referred to the web version of this article.)

0.2 wt%, we estimated the solubility law of CO_2 under dry conditions (pure CO_2) in order to estimate the entrapment pressure of the analysed melt inclusions based on their CO_2 contents (see inset in Fig. 4).

4.3. Melt inclusions in natural feldspar

To untangle the effects of pressure and temperature changes on the anorthoclase composition, we analysed melt inclusions (MI) hosted by the natural anorthoclase crystals. Inclusions are very large (up to 600-μm-across) and tend to be elongated perpendicular to the crystal-growth direction such that they are entrapped in relatively distinct (with respect to composition) growth zones. Melt inclusions rarely contain bubbles but some of the largest MI do. Whether these bubbles are formed by contraction during cooling of the MI or represent gas entrapped at depth is unclear, as bubbles were not analysed. Melt inclusions from five crystals were imaged by X-ray μ-CT (see Methods in Section 2) to ensure their isolation from each other and from the crystal margins (see accompanying video showing the 3D imaging). Fifty-two melt inclusions from four crystals (three of which were imaged by X-ray μ-CT) were then analysed for major elements by EMP analysis, and for volatile contents (CO_2 and H_2O) by SIMS (Table 1; see Methods in Section 2). The major element chemistry of all melt inclusions analysed is fairly uniform. Given the size of the inclusions, and the absence of secondary minerals or any chemical difference with the

Table 1
Volatile contents in melt inclusions determined by SIMS and EMP analysis of melt inclusions. See Table S7 for associated errors.

Crystal	Melt inclusion	CO_2 (ppm)	H_2O (wt%)	Entrapment pressure (MPa)[a]	SiO_2	TiO_2	Al_2O_3	FeO	MnO	MgO	CaO	Na_2O	K_2O	Total	Host zone			Image greyscale[b]
															Ab	An	Or	
Ere_1984_03_S2	Ere_1984_03_S2_02	82	0.10	12	56.47	1.05	19.51	5.23	0.26	0.81	1.78	8.34	6.71	100.15	66.4	13.5	20.0	
	Ere_1984_03_S2_02b	68	0.11	9	56.66	1.02	19.51	5.11	0.25	0.78	1.74	8.29	6.91	100.28	66.2	14.0	19.9	
	Ere_1984_03_S2_03	113	0.09	18	56.19	1.03	19.77	5.18	0.25	0.82	1.89	8.28	6.57	99.98	65.6	17.2	17.1	
	Ere_1984_03_S2_04	132	0.11	21	56.01	0.99	19.85	5.00	0.28	0.80	1.81	8.40	6.85	99.98	65.9	17.0	17.2	
	Ere_1984_03_S2_07	221	0.12	41	56.44	0.98	20.03	5.26	0.28	0.83	1.85	8.36	6.64	100.67	65.9	17.6	16.5	
	Ere_1984_03_S2_11	93	0.12	14	56.15	1.02	19.16	5.30	0.30	0.80	1.73	8.57	7.15	100.18	65.5	13.0	21.5	
	Ere_1984_03_S2_12	277	0.10	55	56.49	1.01	19.60	5.23	0.24	0.81	1.82	8.47	6.91	100.60	66.1	17.8	16.1	
	Ere_1984_03_S2_12b	196	0.10	35	55.77	1.06	19.38	5.31	0.24	0.84	1.14	9.03	7.10	99.87	66.0	15.7	18.3	
	Ere_1984_03_S2_13	137	0.05	22	55.72	1.03	19.66	5.33	0.31	0.83	1.44	8.94	7.02	100.28	65.9	15.6	18.4	
	Ere_1984_03_S2_14	165	0.10	28	56.36	0.97	19.96	5.26	0.28	0.83	1.88	8.32	6.42	100.27	65.9	18.2	16.0	
	Ere_1984_03_S2_15	174	0.09	30	56.08	0.98	19.81	5.20	0.21	0.80	1.82	8.56	6.68	100.14	66.1	17.4	16.5	
	Ere_1984_03_S2_16	180	0.12	32	56.13	0.99	19.91	5.24	0.23	0.82	1.87	8.26	6.76	100.20	66.2	16.0	17.8	
	Ere_1984_03_S2_1b	199	0.10	36	56.51	1.00	19.46	4.99	0.33	0.77	1.73	8.35	6.97	100.11	66.1	15.2	18.7	
Ere_1984_XC_06_S2	Ere_1984_XC_06_S2_01d	289	0.13	58	55.93	1.01	19.35	5.17	0.32	0.83	1.93	8.02	6.03	98.58	66.5	15.2	18.3	
	Ere_1984_XC_06_S2_02	405	0.15	88	56.91	0.99	20.35	4.97	0.26	0.78	1.79	8.26	6.37	100.69	66.2	18.4	15.4	
	Ere_1984_XC_06_S2_04	447	0.12	100	57.20	1.01	19.69	5.22	0.22	0.82	1.91	8.05	6.05	100.18	65.9	14.4	19.7	
	Ere_1984_XC_06_S2_07	431	0.13	96	56.73	1.01	20.05	5.17	0.29	0.80	1.88	7.99	6.21	100.13	66.2	16.7	17.1	
	Ere_1984_XC_06_S2_09	282	0.12	56	57.26	1.01	19.67	5.23	0.26	0.80	1.83	8.15	6.30	100.51	66.2	13.7	20.1	
Ere_2005_042_01_S3	Ere_2005_042_01_S3_01	232	0.10	43	56.69	0.97	19.96	5.07	0.30	0.80	1.88	8.68	6.36	100.72	66.5	16.9	16.6	817
	Ere_2005_042_01_S3_02	274	0.11	54	56.66	0.97	19.88	5.09	0.24	0.82	1.93	8.49	6.38	100.45	66.2	17.1	16.7	758
	Ere_2005_042_01_S3_03	201	0.15	36	56.43	0.96	19.78	5.26	0.28	0.79	1.95	8.48	6.59	100.51	66.5	17.5	15.9	760
	Ere_2005_042_01_S3_06	293	0.12	59	56.71	0.97	19.72	5.28	0.27	0.83	1.99	8.45	6.36	100.59	66.7	16.4	16.9	
	Ere_2005_042_01_S3_07	241	0.12	46	56.49	0.96	19.78	5.05	0.29	0.78	1.87	8.62	6.71	100.54	66.6	15.7	17.8	826
	Ere_2005_042_01_S3_08	279	0.11	55	56.49	1.00	19.58	5.17	0.28	0.84	2.04	8.38	6.38	100.16	66.3	17.5	16.2	764
	Ere_2005_042_01_S3_12	242	0.11	46	56.77	1.00	19.70	5.22	0.26	0.79	1.76	8.47	6.58	100.54	66.5	16.5	17.0	719
	Ere_2005_042_01_S3_15	277	0.12	55	56.67	0.99	19.68	5.10	0.27	0.80	2.00	8.39	6.38	100.27	66.9	17.3	15.9	707
	Ere_2005_042_01_S3_16	230	0.13	43	56.61	1.01	19.87	5.34	0.30	0.77	1.98	8.50	6.21	100.59	66.3	17.5	16.2	732
	Ere_2005_042_01_S3_21	249	0.11	48	56.38	1.01	19.84	5.36	0.29	0.84	2.01	8.27	6.15	100.16	66.0	16.9	17.1	
	Ere_2005_042_01_S3_22	215	0.12	40	56.39	0.99	19.91	5.29	0.23	0.79	1.91	8.37	6.58	100.46	66.3	16.9	16.8	728
	Ere_2005_042_01_S3_23	172	0.10	30	56.45	0.97	19.72	5.23	0.27	0.80	1.98	8.14	6.41	99.96	66.3	17.3	16.4	833
	Ere_2005_042_01_S3_24	363	0.13	77	56.67	0.95	19.78	5.16	0.29	0.88	1.99	8.45	6.35	100.53	66.5	17.5	16.0	
	Ere_2005_042_01_S3_25	310	0.11	63	56.65	1.00	19.92	5.16	0.23	0.77	1.87	8.63	6.66	100.88	66.7	16.1	17.2	710
	Ere_2005_042_01_S3_26	241	0.13	46	56.63	0.99	19.69	5.15	0.26	0.81	1.96	8.36	6.47	100.34	66.4	17.3	16.3	
eb05027a2	eb05027a2_01	251	0.14	48	56.46	1.00	20.31	5.22	0.26	0.78	1.84	7.96	6.21	100.05	65.3	16.8	17.9	65.20
	eb05027a2_02	232	0.12	44	56.24	0.98	20.35	5.05	0.24	0.79	1.91	8.12	6.10	99.79	65.0	17.3	17.8	63.60
	eb05027a2_03	270	0.14	53	56.22	1.04	19.99	5.07	0.31	0.86	1.93	7.85	6.25	99.53	65.0	15.5	19.5	68.80
	eb05027a2_04	231	0.13	43	56.43	0.96	20.14	5.13	0.24	0.83	1.94	7.98	6.05	99.68	65.7	14.6	19.7	71.16
	eb05027a2_05	232	0.13	44	56.19	0.99	20.02	5.22	0.28	0.85	1.93	7.91	6.13	99.51	65.8	15.7	18.5	67.10
	eb05027a2_06	204	0.12	37	56.19	1.02	20.13	5.16	0.31	0.83	1.94	8.00	6.16	99.73	65.4	15.5	19.1	65.00
	eb05027a2_07	266	0.12	52	56.57	0.95	20.30	4.83	0.22	0.80	1.81	8.03	6.34	99.85	65.6	17.1	17.3	64.00
	eb05027a2_09	294	0.15	59	56.27	1.06	20.02	5.24	0.31	0.84	1.97	8.08	6.16	99.94	65.6	15.8	18.6	66.40
	eb05027a2_10	239	0.13	45	56.39	1.00	20.15	4.97	0.21	0.81	1.89	7.60	6.31	99.34	65.2	13.7	21.1	73.50
	eb05027a2_11	175	0.11	30	56.30	0.94	20.24	4.91	0.24	0.79	1.88	8.00	6.29	99.57	65.1	15.1	19.8	70.00
	eb05027a2_12	216	0.11	40	56.39	0.93	20.21	5.02	0.33	0.83	1.90	8.01	6.25	99.86	65.6	15.0	19.4	70.00
	eb05027a2_13	261	0.11	51	56.26	0.96	20.07	4.98	0.32	0.82	1.82	8.04	6.13	99.40	65.2	13.8	21.0	73.05
	eb05027a2_14	248	0.12	47	56.43	1.03	20.10	5.24	0.28	0.79	1.91	7.93	6.19	99.91	65.2	14.3	20.5	71.10
	eb05027a2_15	153	0.12	26	56.30	0.98	20.13	5.00	0.25	0.80	1.95	7.73	6.34	99.49	65.4	14.3	20.3	75.70
	eb05027a2_18	436	0.15	97	56.14	1.01	20.27	5.26	0.25	0.82	1.87	8.34	6.19	100.16	65.6	17.0	17.5	64.00
	eb05027a2_19	292	0.12	58	55.81	1.07	20.37	5.30	0.24	0.86	1.80	8.08	6.29	99.81	65.4	16.6	18.0	62.60
	eb05027a2_20	290	0.12	58	56.24	0.93	20.43	4.97	0.21	0.80	1.76	8.08	6.19	99.61	65.9	16.1	18.0	65.80
	eb05027a2_22	217	0.11	40	55.97	1.01	20.37	5.11	0.32	0.86	1.99	8.26	6.37	100.25	65.7	16.0	18.3	67.70
	eb05027a2_24	217	0.11	40	56.40	1.09	19.66	5.56	0.27	0.89	1.94	7.84	6.13	99.78	65.4	13.4	21.2	80.7
eb05027a2	eb05027a2_GL01	96	0.05	14	57.18	1.04	19.69	5.29	0.28	0.85	1.92	8.28	6.03	100.57	64.2	11.7	24.1	86.00
	eb05027a2_GL02	52	0.07	7	57.24	0.97	19.95	5.20	0.27	0.77	1.78	7.98	6.30	100.46	64.9	12.8	22.3	88.00
	eb05027a2_GL03	29	0.07	3	56.63	1.01	19.72	5.29	0.29	0.82	1.83	8.02	6.17	99.77	64.5	11.3	24.2	88.00

[a] Pressure calculated using equation from Fig. 4. The relative error on the entrapment pressure is 6.3% if calculated from a 5% relative error on the CO_2 measurement. While error associated with the equation from Fig. 4 cannot be quantified, the error on the pre-power term would have no effect and a 15% error on the exponent value would affect the entrapment pressure's relative error by 1%.

[b] Undetermined greyscale values for crystal Ere_2005_042_01_S3 are due to uneven sample thickness skewing the image brightness.

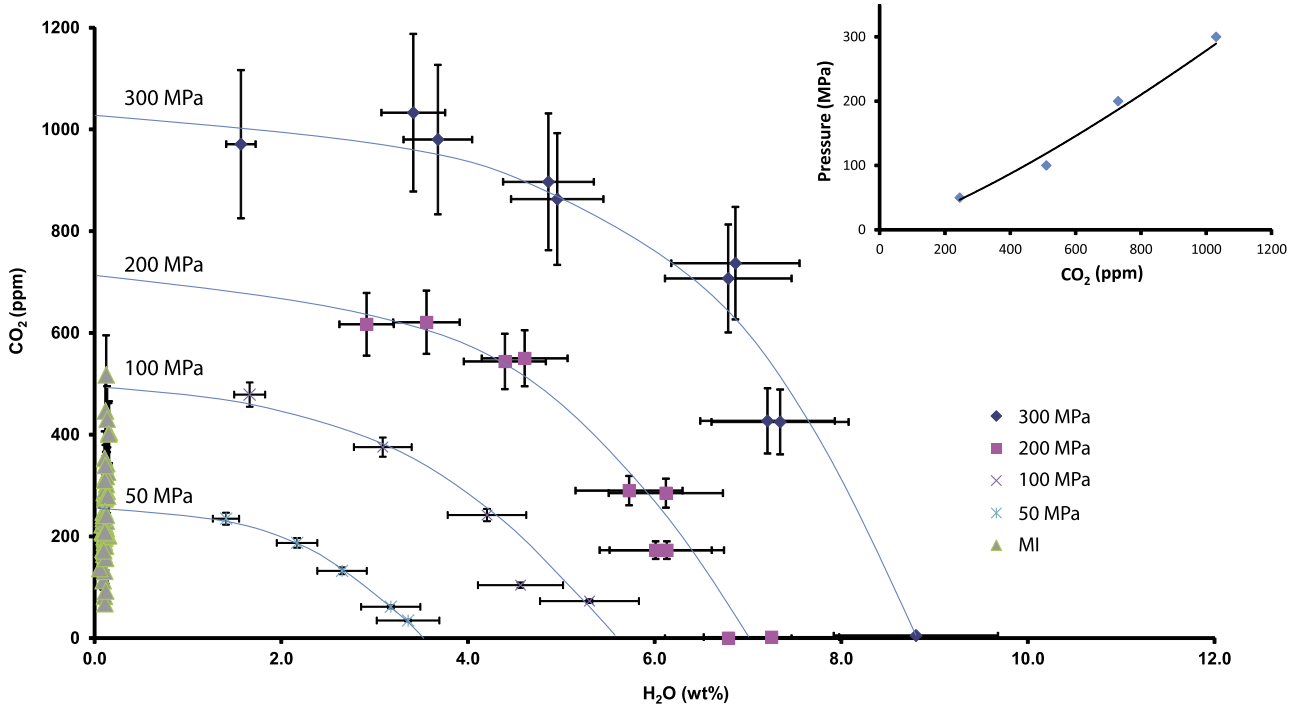

Fig. 4. Results of solubility experiments from Erebus phonolite between 50 and 300 MPa. Volatile contents of all melt inclusion from anorthoclase crystals analysed in this study (and additional unpublished data) are also plotted. Error from SIMS analysis is estimated at 15%. Inset: CO_2 solubility in Erebus phonolite estimated for $H_2O = 0$ wt%. The best fit line ($R^2 = 0.98$) has the following equation: $P_{(MPa)} = 0.0433(CO_2)^{1.2696}$.

matrix glass, we did not attempt corrections for post-entrapment processes.

The composition of the host zone was characterized in two ways: (i) from the average greyscale value of the pixels surrounding the inclusion in potassium X-ray maps (Fig. 1), providing a qualitative estimate of the variation in Or content; and (ii) by averaging three EMP analyses of the natural anorthoclase directly surrounding each inclusion (Fig. 5). Both approaches identify a relationship between entrapment depth of a given melt inclusion and the chemistry of its host zone: inclusions entrapped at higher pressure (i.e., higher CO_2 content) tend to be located within comparatively orthoclase-poor zones (darker zones with lower greyscale values in the X-ray maps).

While the melt inclusion data tend to follow the experimental isothermal trends, some scatter is apparent, suggesting that the temperature of the natural system might vary slightly between 950 and 975 °C (Fig. 5). To a first order, these findings corroborate the experimental results in defining a relationship between the chemistry of a crystal zone and its growth pressure, and preclude the explanation that the oscillatory zoning in the natural anorthoclase might arise from boundary layer processes. Moreover, the MgO content of the melt is a function of the temperature as determined by experiments (Moussallam et al., 2013; Fig. 6, and Fig. S2 in Supplementary Information). The absence of correlation between an inclusion's MgO content and the chemistry of its host zone, and indeed the absence of any variation in the inclusions' MgO and FeO content, strongly argues against large temperature variations or episodic mafic input affecting the system. All the analysed natural feldspars essentially grew from the same, near isothermal, phonolitic melt.

In summary, glass and melt inclusions hosted in anorthoclase zones of variable composition (16–24% Or), show (i) little variation in water content (0.05–0.15 wt%), (ii) little variation in major element chemistry (e.g. MgO, 0.77–0.89 wt%), but (iii) variation in CO_2 content (30–450 ppm) corresponding to a wide range of entrapment pressure (3–100 MPa). The correspondence between the host-zone chemistry and melt inclusion-entrapment pressure, together with the lack of correlation between the host-zone chemistry with either MgO or H_2O contents, argues that the natural anorthoclase chemical zoning is best interpreted as a record of growth at variable pressure (i.e. depth).

4.4. Tracking magma motion and speed

Using the experimentally-determined synthetic feldspar chemistry relationship at 950 °C and 975 °C (Fig. 5), we computed the expected relationship at 962 °C, the temperature that best reproduces the natural system (Fig. S3 in Supplementary Information). We then converted rim-to-rim and core-to-rim transects of orthoclase content of the natural anorthoclase crystals (Figs. 1 and 2) to temporal profiles of the pressure (i.e. depth) of crystal growth (Fig. 7). Further transects are shown in Fig. 8 and suggest that, at greater depths, crystals are subjected to depth oscillations of large amplitude and high frequency, whereas closer to the surface, the depth variations are of lesser amplitude and are more irregular in time. This may reflect contrasting fluid dynamics in the magma reservoir compared with the exchange flow prevailing in the conduit. Based on these contrasting regimes, we assigned the first 20 MPa to represent the conduit (a length of ~750 m) and lava lake (depth of a few tens of meter), and a magmatic reservoir with distinct geometry and/or dynamic regime at higher pressure (20–200 MPa). This magma plumbing geometry is broadly consistent with the failure of seismological techniques to detect any sizeable magmatic reservoir in the first kilometer below the summit (Zandomeneghi et al., 2013).

With this conceptual model in mind, Fig. 7 retraces the growth history of a natural anorthoclase crystal, and the multiple journeys it made on the "magma conduit elevator" between a putative magma reservoir and the lava lake, until it was eventually expelled in a lava bomb by an explosion in 2005. Other profiled natural anorthoclase crystals (Fig. 8) provide additional records of crys-

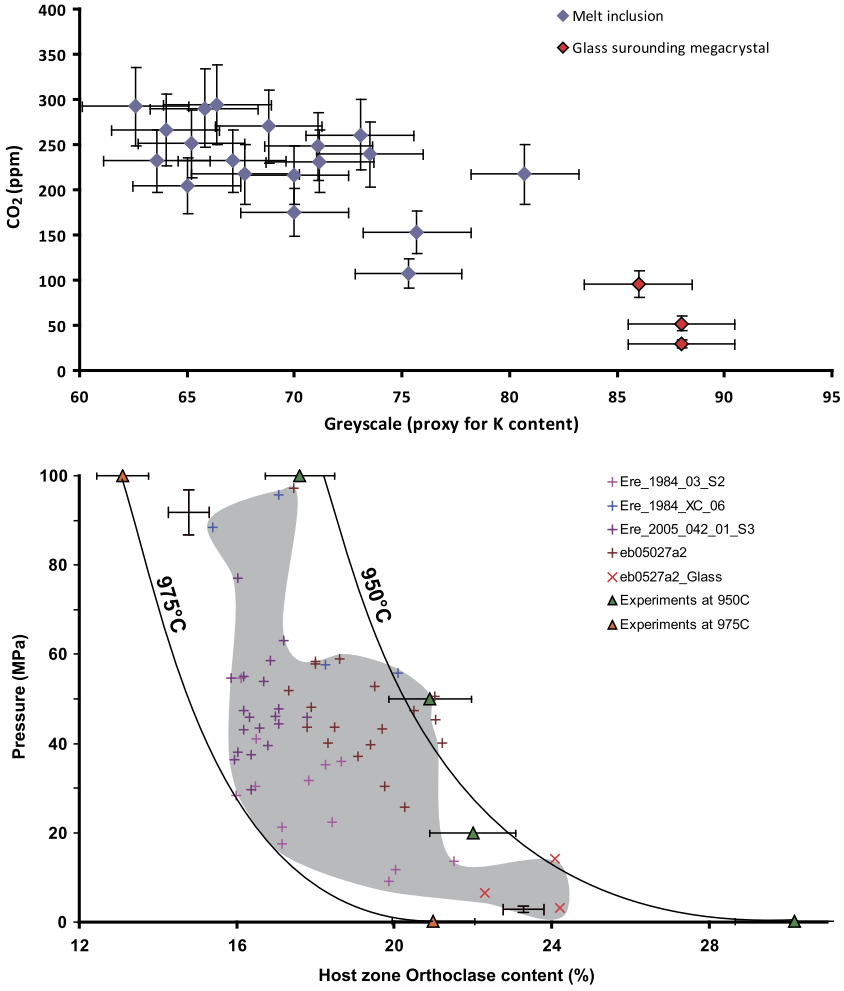

Fig. 5. Upper plot: CO_2 contents of melt inclusions and glass in contact with the rim of crystal *eb05027a2* plotted against the average greyscale value of the pixel surrounding the inclusion, obtained from the potassium X-ray map (Fig. 1). In the case of the matrix glass, the average value for the immediate region beyond the crystal edge was calculated. Lower plot: entrapment pressures of melt inclusions from four crystals, plotted against the orthoclase content of their host zone as determined from EMP analyses. Experimental anorthoclase compositions are also plotted for experiments conducted at 950 and 975 °C and for a range of pressure. Errors are reported in Table S7. Errors on Or content of synthetic anorthoclase are plotted for each experiment; representative error on MI entrapment pressure and Or content from host zone are also shown, bracketing the data.

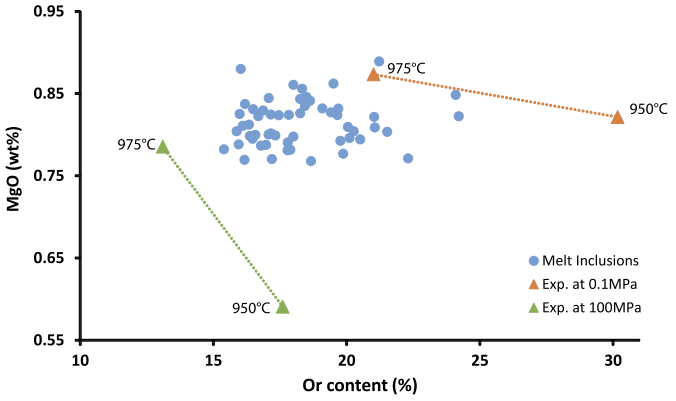

Fig. 6. Expected relationship between MgO content of the melt and feldspar chemistry (express as Orthoclase content) from experiments at 0.1 and 100 MPa (Moussallam et al., 2013) and MgO content of MI analysed. Note the absence of relationship between the MI MgO contents and the chemistry of the zone in which the inclusions are entrapped.

tal ascent and descent consistent with a bi-directional flow regime (Huppert and Hallworth, 2007; Oppenheimer et al., 2009).

The mean density of the anorthoclase crystals can be estimated at 2524 kg m^{-3} (using measured value of 2590 kg m^{-3} at room temperature and calculated at 962 °C using the volumetric thermal expansion coefficient from Hovis et al., 2010), while the phonolite melt density is estimated at 2333 kg m^{-3} (calculated at 962 °C using partial molar volumes from Bottinga and Weill, 1970). Given the density contrast between the anorthoclase crystals and the phonolitic melt, settling of the anorthoclase crystals is expected (Molina et al., 2012). Multiple lines of evidence however, suggest otherwise. Firstly, the uniform chemistry of the lava erupted over the last ~20 ka and the constant proportion of anorthoclase crystals (~30 vol%) in these lava (Kelly et al., 2008) argues against removal of anorthoclase over time. Secondly, anorthoclase crystal size distributions in volcanic bombs show a linear relationship between the natural logarithm of the crystal number density (as a function of linear crystal size) and crystal width, and no accumulation in the larger size classes. This suggests that crystallisation has been continuous through time and that accumulation of anorthoclase crystals has not been an important factor in generating Erebus lavas (Dunbar et al., 1994).

We also note that the anorthoclase crystals cannot be derived from a mush layer since any concentration of crystals greater than 30 vol% modal is only stable below 925 °C, in equilibrium with biotite (a phase never observed in any Erebus lava). Finally, the upper two profiles in Fig. 8 show very similar growth history and are from two anorthoclase crystals taken from the same bomb

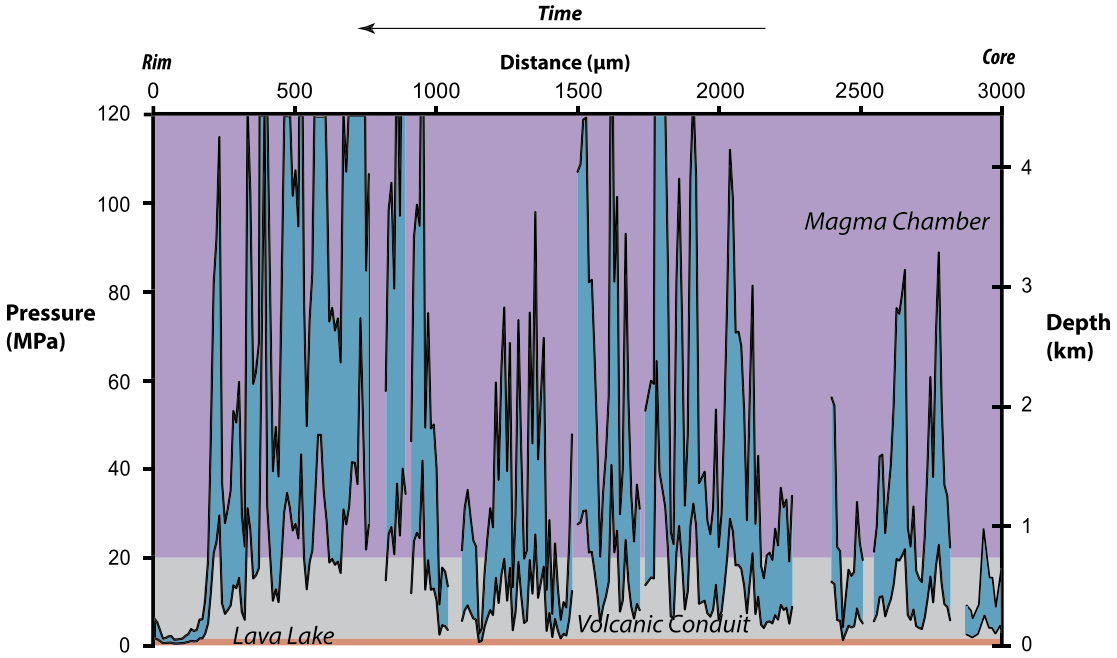

Fig. 7. Estimated growth pressure (and corresponding depth) based on the first 3 mm of the EMP transect of anorthoclase crystal eb05027a2 shown in Fig. 1 and translated to growth pressure using the relationship given in Fig. S3. Depth ranges inferred for the reservoir, conduit and lava lake are shown. The pressure estimate at each point is reported as the 71% confidence interval region estimated using deviations from the equation at 962.5 °C presented in Fig. S3, so as to bracket 71% of the MI data shown in the lower panel of Fig. 5. We note that this error interval is equivalent to the effect of temperature oscillations of ±6.25 °C on the estimated growth pressure. The depth profile is subdivided in zones to represent the magma chamber (lilac), conduit (grey) and lava lake (red). The full profile is shown in Fig. 8 (third panel) with corresponding confidence intervals reported in Fig. S5. (For interpretation of the references to colour in this figure legend, the reader is referred to the web version of this article.)

(erupted in 1984, the other two profiles are from crystals in two different bombs erupted in 2005). This similarity suggests that the two crystals have been travelling within the same coherent batch of magma for an extended period of time spanning numerous up-and-down cycles. Thus the anorthoclase crystals do appear to travel with the magma and track its motion through time, suggesting convection rates and effective viscosities sufficient to keep them in suspension. Le Losq et al. (2015) have computed a viscosity of the order of 10^6 Pa s for Erebus phonolite at 950 °C (i.e., orders of magnitude higher than viscosities of mafic lava lakes such as found at Kīlauea volcano, Hawaii). Such high viscosity will hinder separation of crystals from melt.

We can estimate growth rates of anorthoclase crystals as a function of pressure and temperature from our experimental data (Fig. S6 in Supplementary Information), since the experiment durations are known and the synthetic feldspar crystal size can be measured from SEM images. Crystal growth rates depend largely, for low viscosity melts, on the degree of undercooling of the liquid (Pupier et al., 2008), and we therefore stress that our values can only represent maximum rates. Given that temperature variations are likely to be small, we fix the melt temperature at 962 °C so as to convert zone widths to timescales (Fig. 9). This suggests that vertical speeds within the magma chamber (about 0.3–1 mm s^{-1}) are up to an order of magnitude greater than in the conduit (where they are about 0.1–0.2 mm s^{-1}). The vertical speed in the magma chamber suggests a Rayleigh number, Ra, of order 10^{17} (based on an average ascent speed of 0.5 mm s^{-1} and a 1-km-deep chamber, and using Eq. (8) in Snyder (2000), and the relevant parameters given in Table S9 in the Supplementary Information). The corresponding period of the up-and-down convection cycles in the reservoir is approximately 100–200 days. Such vigorous convection should maintain geochemical homogeneity in the magmatic system, consistent with absence of compositional changes in lavas erupted at Erebus over the last 20 ka (Kelly et al., 2008). Huber et al. (2009) estimated that a minimum of 5–10 overturns are required to achieve reservoir homogenisation in systems of comparable rheology.

The growth rate model also suggests that crystal ages must exceed a few years for the smallest crystals and a hundred years for the largest ones. The relatively small crystal shown in Fig. 1, for instance, must be at least 11 years old. These estimates of crystal ages, based on experimentally-determined growth rates of synthetic feldspar, neglect resorption episodes, which are evident in the crystals. Resorption can arise via two processes: (i) extrinsic changes that move the system outside the experimentally-determined stability field, such as a heating episode that increases temperature above 975 °C; and (ii) Ostwald ripening, in which growth of one crystal occurs at the expense of another. Lacking constraints on the durations of episodic resorption, we cannot constrain upper bounds of crystal ages.

5. Discussion

A prior study (Sumner, 2007), which was based on diffusion modelling and measured Sr and Ba profiles in five natural anorthoclase crystals from Erebus (one of which we have examined here), suggested an average growth rate of 1.4×10^{-9} cm s^{-1}. This is similar to the one we compute for growth of anorthoclase at 962.5 °C and very low pressure (1 MPa). However, the Sr–Ba based estimate is biased by a single outlier, which, if removed, drops the growth rate to 2.1×10^{-10} cm s^{-1}. This is in turn comparable to our estimated growth rate at 100 MPa and to estimates of plagioclase growth rate in other igneous systems (Cashman, 1990). While this does not provide a firm validation of our experimental measurements, the general agreement between rates computed from two independent methods does lend confidence to the conclusions drawn. We also note that, in Fig. 9, crystal *eb*05027*a*2 from a lava bomb erupted on 24 December 2005 appears to have spent its final three months or so in the lava lake. This estimate is compatible with an 80-day-degassing period estimated from U-, Th-series dis-

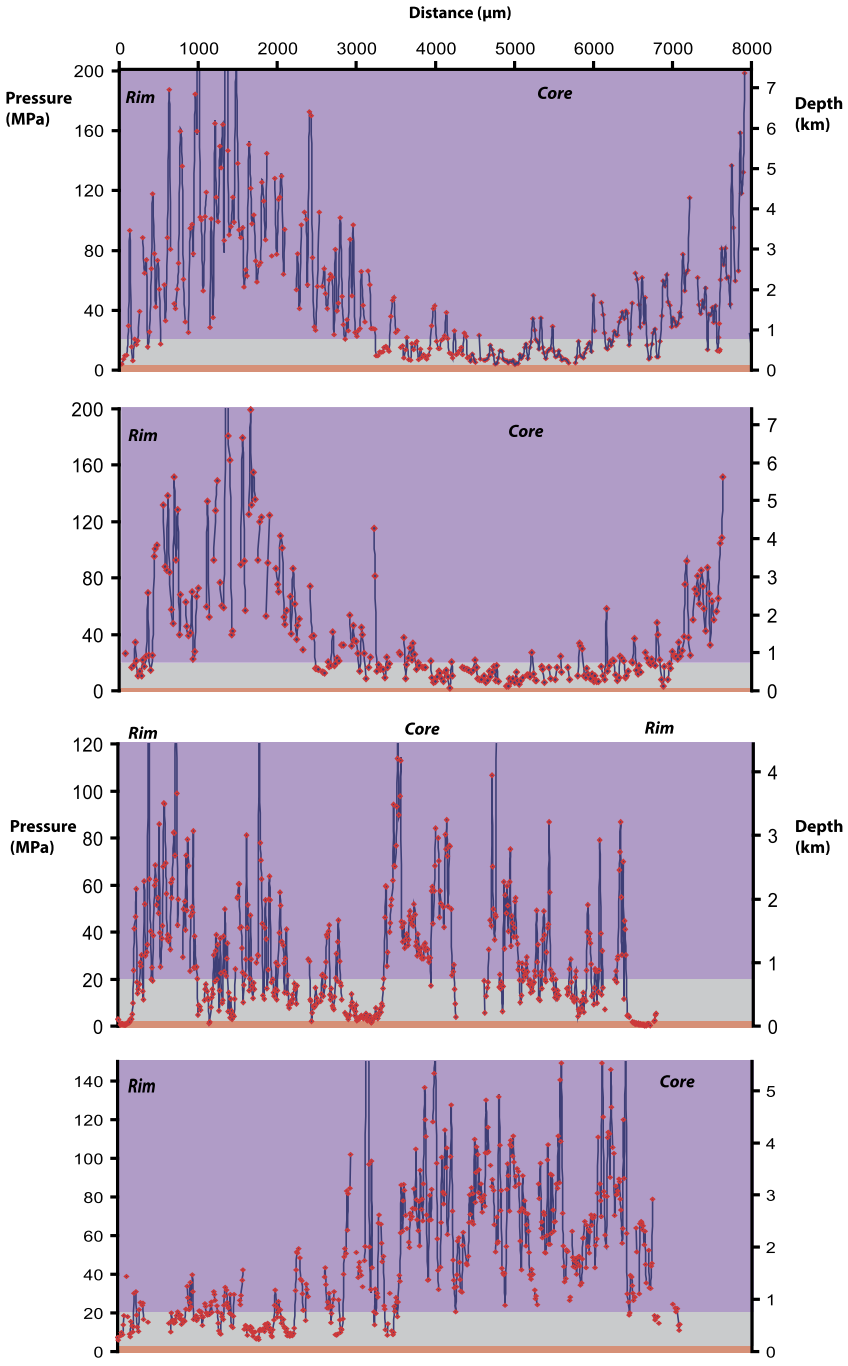

Fig. 8. EMP analysis transects recast in term of estimated growth pressure and depth, calculated from the relation given in Fig. S3. Samples (from top to bottom): Ere_1984_03_S2, Ere_1984_XC_06_S2, eb05027a2 and eb05042b2. Error estimates are shown in Fig. S5. For explanation of colour scheme see caption to Fig. 7. (For interpretation of the references to colour in this figure legend, the reader is referred to the web version of this article.)

equilibria measured for another phonolitic bomb erupted from the lava lake eight days earlier (Sims et al., 2012).

Conduit convection associated with passive degassing and negligible net eruption of lava or tephra beyond the lava lake has been argued to imply that degassed magma is ultimately stored within the crust (Francis et al., 1993; Allard, 1997). This interpretation is only valid, however, if the descending magma remains degassed. At Erebus, the crystal record provides evidence that the magma undergoes multiple journeys back-and-forth between the magma chamber and the near surface. Degassed magma therefore has the opportunity to remix at depth and carry a new batch of volatiles (essentially CO_2, but some H_2O also) back to the surface. This process is driven by the sustained CO_2 flux originating from the deeper basanitic reservoir in contact with the mantle source region (Oppenheimer et al., 2011; Moussallam et al., 2013). The ubiquitously dry nature of Erebus phonolitic magma (<0.2 wt%), very close to its degassed value in the lava lake (~0.05 wt%) and much lower than the parental basanite (~1–2 wt%; Eschenbacher, 1998), suggests that it is the CO_2 fluxing that sustains convection of the phonolitic system by allowing the degassed, sinking magma to recharge with volatiles and deliver them to the surface.

The continuous degassing of not only CO_2 but also significant amounts of H_2O results in the progressive dehydration of the phonolitic magma. We suggest that such a magma plumbing architecture can maintain an effective pathway for deep volatiles to reach the surface without requiring crustal accumulation of

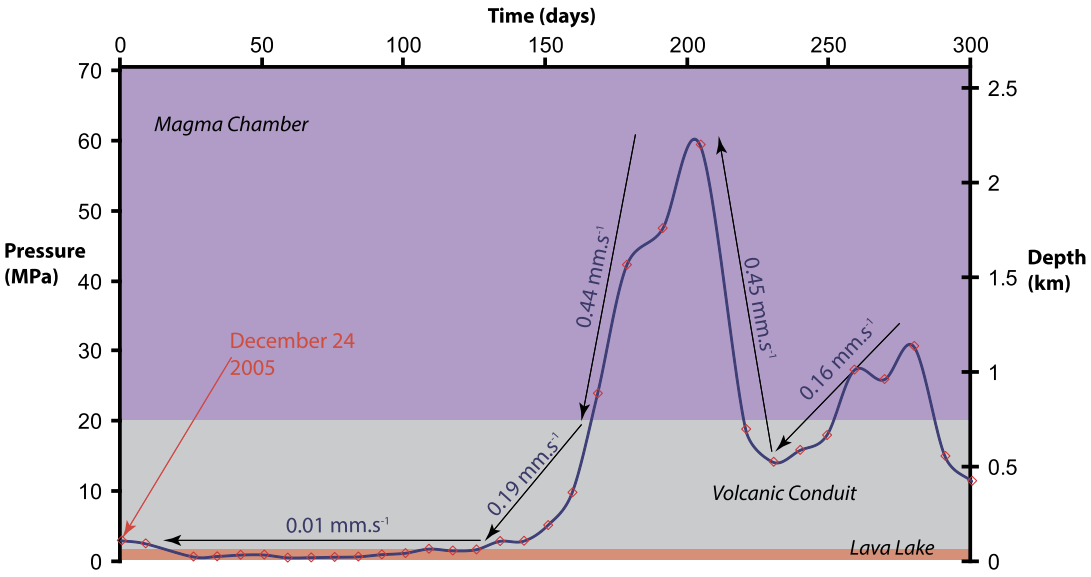

Fig. 9. Closer view of the growth pressure *vs.* time history for the outer part of the crystal presented in Fig. 7. The vertical speed is shown for portions of the transect. Note that since experimentally determined crystal growth rates can only be considered as maximum values, the *x*-axis represents minimum time before eruption and the vertical speed is a maximum estimate. For explanation of colour scheme see caption to Fig. 7.

magma. Emplacement of mafic magma in the lower crust is therefore likely to be more significant volumetrically than endogenous growth of the volcanic edifice (Francis et al., 1993).

6. Conclusions

We have investigated the origin of oscillatory zoning in anorthoclase megacrysts from Erebus volcano by means of phase equilibrium, solubility experiments and an analysis of melt inclusion data. We have found that the chemical profiles are best explained by growth at variable pressure (i.e. depth). The key conclusions we draw from our findings are:

i. Anorthoclase crystals track substantial magma transport between the surface lava lake and reservoir via the conduit. This finding corroborates the idea of conduit convection, supported by laboratory analogue models that reproduce bi-directional flow, and interpretation of gas, thermal and cosmic-ray muon radiography observations (Shinohara et al., 1995; Huppert and Hallworth, 2007; Beckett et al., 2011; Oppenheimer et al., 2011; Shinohara and Tanaka, 2012) made at a number of quiescently degassing ('open-vent') volcanoes.
ii. The large amplitude and high frequency cyclic oscillations (periodicity of ~150 days) recorded by the crystals at depth argue for a vertically extensive (several kilometers) and vigorously convecting reservoir. Crystals appear to have spent longer time intervals in the reservoir than in the conduit and lava lake where vertical motion is more complex due to the proximity of upwelling and downwelling flows and the potential for recurrent re-entrainment into the opposing flow.
iii. A typical crystal, 1-cm-across may be at least 14 years old and may have made several (~1–3) complete journeys up and down the conduit. This suggests that magma reaching the lava lake will degas and sink, but eventually (and it is not clear how fast) re-incorporate volatiles, to the point of rising again and repeating the cycle. This continuous motion may be sustained by the constant fluxing of CO_2 sourced from a deeper basanitic reservoir, degassing over time and accumulating within the lower crust, while the upper phonolitic magma is constantly recycled, kept in motion and progressively dehydrated.

Acknowledgements

We thank Ida Di Carlo, Rémi Champallier, Marina Alletti, Mickael Laumonier, Giada Iacono Marziano and David Sifre for assistance in the laboratory. The work reported here has been partially supported by the National Science Foundation (Division of Polar Programs) under grant ANT1142083. The authors thank the Natural Environment Research Council (NERC) for access to the NERC Ion Microprobe Facility (Grant IMF453/1011) and Richard Hinton for invaluable help with SIMS analyses. Y.M. acknowledges support from the Cambridge Philosophical Society, the University of Cambridge Home and EU Scholarship Scheme, and the Philip Lake and William Vaughan Lewis funds from the Department of Geography, University of Cambridge. Y.M. also acknowledges support from ERC grant #279790. Valuable reviews by three anonymous reviewers and Tim Elliott improved the quality of the manuscript.

Appendix A. Supplementary material

Supplementary material related to this article can be found online at http://dx.doi.org/10.1016/j.epsl.2014.12.022.

References

Allard, P., 1997. Endogenous magma degassing and storage at Mount Etna. Geophys. Res. Lett. 24 (17), 2219–2222. http://dx.doi.org/10.1029/97GL02101.

Allegre, C., Provost, A., Jaupart, C., 1981. Oscillatory zoning: a pathological case of crystal growth. Nature 294 (5838), 223–228. http://dx.doi.org/10.1038/294223a0.

Beckett, F.M., Mader, H.M., Phillips, J.C., Rust, A.C., Witham, F., 2011. An experimental study of low-Reynolds-number exchange flow of two Newtonian fluids in a vertical pipe. J. Fluid Mech. 682, 652–670. http://dx.doi.org/10.1017/jfm.2011.264.

Bottinga, Y., Weill, D.F., 1970. Densities of liquid silicate systems calculated from partial molar volumes of oxide components. Am. J. Sci. 269 (2), 169–182.

Bowen, N.L., 1928. The Evolution of the Igneous Rocks. Princeton University.

Cashman, K.V., 1990. Textural constraints on the kinetics of crystallization of igneous rocks. Rev. Mineral. Geochem. 24 (1), 259–314.

Charlier, B.L.A., Wilson, C.J.N., Davidson, J.P., 2008. Rapid open-system assembly of a large silicic magma body: time-resolved evidence from cored plagioclase crystals in the Oruanui eruption deposits, New Zealand. Contrib. Mineral. Petrol. 156 (6), 799–813. http://dx.doi.org/10.1007/s00410-008-0316-y.

Di Carlo, I., Pichavant, M., Rotolo, S.G., Scaillet, B., 2006. Experimental crystallization of a high-K arc basalt: the Golden Pumice, Stromboli Volcano (Italy). J. Petrol. 47 (7), 1317–1343.

Dunbar, N.W., Cashman, K., Dupre, R., 1994. Crystallization processes of anorthoclase phenocrysts in the Mount Erebus magmatic system: evidence from crystal composition, crystal size distributions and volatile contents of melt inclusions. In: Kyle, Philip R. (Ed.), Volcanological and Environmental Studies of Mt. Erebus, Antarctica. In: Antarct. Res. Ser., vol. 66, pp. 129–146.

Eschenbacher, A., 1998. Open-system degassing of a fractionating, alkaline magma, Mount Erebus, Ross Island, Antarctica. Unpublished Master's thesis. New Mexico Institute of Mining and Technology, Socorro.

Francis, P., Oppenheimer, C., Stevenson, D., 1993. Endogenous growth of persistently active volcanoes. Nature 366 (6455), 554–557. http://dx.doi.org/10.1038/366554a0.

Ginibre, C., Wörner, G., Kronz, A., 2007. Crystal zoning as an archive for magma evolution. Elements 3 (4), 261–266. http://dx.doi.org/10.2113/gselements.3.4.261.

Harloff, C., 1927. Zonal structure in plagioclase. In: Leidsche Geologische Medelelingen, pp. 99–114.

Hovis, G.L., Medford, A., Conlon, M., Tether, A., Romanoski, A., 2010. Principles of thermal expansion in the feldspar system. Am. Mineral. 95 (7), 1060–1068.

Huber, C., Bachmann, O., Manga, M., 2009. Homogenization processes in silicic magma chambers by stirring and mushification (latent heat buffering). Earth Planet. Sci. Lett. 283 (1–4), 38–47. http://dx.doi.org/10.1016/j.epsl.2009.03.029.

Humphreys, M.C.S., Blundy, J.D., Sparks, R.S.J., 2006. Magma evolution and open-system processes at Shiveluch Volcano: insights from phenocryst zoning. J. Petrol. 47 (12), 2303–2334. http://dx.doi.org/10.1093/petrology/egl045.

Huppert, H.E., Hallworth, M.A., 2007. Bi-directional flows in constrained systems. J. Fluid Mech. 578, 95–112. http://dx.doi.org/10.1017/S0022112007004661.

Kahl, M., Chakraborty, S., Costa, F., Pompilio, M., Liuzzo, M., Viccaro, M., 2013. Compositionally zoned crystals and real-time degassing data reveal changes in magma transfer dynamics during the 2006 summit eruptive episodes of Mt. Etna. Bull. Volcanol. 75 (2), 1–14. http://dx.doi.org/10.1007/s00445-013-0692-7.

Kazahaya, K., Shinohara, H., Saito, G., 1994. Excessive degassing of Izu-Oshima volcano: magma convection in a conduit. Bull. Volcanol. 56 (3), 207–216. http://dx.doi.org/10.1007/BF00279605.

Kelly, P.J., Kyle, P.R., Dunbar, N.W., Sims, K.W.W., 2008. Geochemistry and mineralogy of the phonolite lava lake, Erebus volcano, Antarctica: 1972–2004 and comparison with older lavas. J. Volcanol. Geotherm. Res. 177 (3), 589–605.

Kyle, P.R., 1977. Mineralogy and glass chemistry of recent volcanic ejecta from Mt. Erebus, Ross Island, Antarctica. N.Z. J. Geol. Geophys. 20, 1123–1146.

Kyle, P.R., Moore, J.A., Thirlwall, M.F., 1992. Petrologic evolution of anorthoclase phonolite lavas at Mount Erebus, Ross Island, Antarctica. J. Petrol. 33 (4), 849–875.

L'Heureux, I., Fowler, A., 1996. Dynamical model of oscillatory zoning in plagioclase with nonlinear partition relation. Geophys. Res. Lett. 23 (1), 17–20. http://dx.doi.org/10.1029/95GL03327.

Le Losq, C., Neuville, D.R., Moretti, R., Kyle, P.R., Oppenheimer, C., 2015. Rheology of phonolite magmas – the case of the Erebus lava lake. Earth Planet. Sci. Lett. 411, 53–61. http://dx.doi.org/10.1016/j.epsl.2014.11.042.

Molina, I., Burgisser, A., Oppenheimer, C., 2012. Numerical simulations of convection in crystal-bearing magmas: a case study of the magmatic system at Erebus, Antarctica. J. Geophys. Res. 117 (B7), B07209. http://dx.doi.org/10.1029/2011JB008760.

Moussallam, Y., Oppenheimer, C., Scaillet, B., Kyle, P.R., 2013. Experimental phase-equilibrium constraints on the phonolite magmatic system of Erebus Volcano, Antarctica. J. Petrol.. http://dx.doi.org/10.1093/petrology/egt012.

Oppenheimer, C., Lomakina, A.S., Kyle, P.R., Kingsbury, N.G., Boichu, M., 2009. Pulsatory magma supply to a phonolite lava lake. Earth Planet. Sci. Lett. 284 (3–4), 392–398.

Oppenheimer, C., Moretti, R., Kyle, P.R., Eschenbacher, A., Lowenstern, J.B., Hervig, R.L., Dunbar, N.W., 2011. Mantle to surface degassing of alkalic magmas at Erebus volcano, Antarctica. Earth Planet. Sci. Lett. 306 (3–4), 261–271. http://dx.doi.org/10.1016/j.epsl.2011.04.005.

Pupier, E., Duchene, S., Toplis, M.J., 2008. Experimental quantification of plagioclase crystal size distribution during cooling of a basaltic liquid. Contrib. Mineral. Petrol. 155 (5), 555–570. http://dx.doi.org/10.1007/s00410-007-0258-9.

Scaillet, B., Pichavant, M., Roux, J., Humbert, G., Lefèvre, A., 1992. Improvement of the Shaw membrane technique for measurement and control of fH_2 at high temperatures and pressures. Am. Mineral. 77, 617–655.

Shinohara, H., Tanaka, H.K.M., 2012. Conduit magma convection of a rhyolitic magma: constraints from cosmic-ray muon radiography of Iwodake, Satsuma-Iwojima volcano, Japan. Earth Planet. Sci. Lett. 349–350, 87–97. http://dx.doi.org/10.1016/j.epsl.2012.07.002.

Shinohara, H., Kazahaya, K., Lowenstern, J.B., 1995. Volatile transport in a convecting magma column: implications for porphyry Mo mineralization. Geology 23 (12), 1091–1094. http://dx.doi.org/10.1130/0091-7613(1995)023<1091:vVTIACM>2.3.CO;2.

Shore, M., Fowler, A., 1996. Oscillatory zoning in minerals; a common phenomenon. Can. Mineral. 34 (6), 1111–1126.

Sims, K.W.W., Pichat, S., Reagan, M.K., Kyle, P.R., Dulaiova, H., Dunbar, N.W., Prytulak, J., Sawyer, G., Layne, G.D., Blichert-Toft, J., Gauthier, P.J., Charette, M.A., Elliott, T.R., 2012. On the time scales of magma genesis, melt evolution, crystal growth rates and magma degassing in the Erebus volcano magmatic system using the ^{238}U, ^{235}U and ^{232}Th decay series. J. Petrol 54 (2), 235–271. http://dx.doi.org/10.1093/petrology/egs068.

Singer, B., Dungan, M., Layne, G., 1995. Textures and Sr, Ba, Mg, Fe, K and Ti compositional profiles in volcanic plagioclase clues to the dynamics of calc-alkaline magma chambers. Am. Mineral. 80 (7–8), 776–798.

Snyder, D., 2000. Thermal effects of the intrusion of basaltic magma into a more silicic magma chamber and implications for eruption triggering. Earth Planet. Sci. Lett. 175 (3–4), 257–273. http://dx.doi.org/10.1016/S0012-821X(99)00301-5.

Stevenson, D.S., Blake, S., 1998. Modelling the dynamics and thermodynamics of volcanic degassing. Bull. Volcanol. 60 (4), 307–317. http://dx.doi.org/10.1007/s004450050234.

Sumner, C.L.K., 2007. Residence time estimates and controls on crystallization patterns for anorthoclase phenocrysts in phonolite magma, Erebus volcano, Antarctica. Unpublished Master's Thesis. New Mexico Institute of Mining and Technology, Socorro. Available at: http://www.ees.nmt.edu/outside/alumni/papers/2007t_sumner_cl.pdf.

Viccaro, M., Giacomoni, P.P., Ferlito, C., Cristofolini, R., 2010. Dynamics of magma supply at Mt. Etna volcano (Southern Italy) as revealed by textural and compositional features of plagioclase phenocrysts. Lithos 116 (1–2), 77–91. http://dx.doi.org/10.1016/j.lithos.2009.12.012.

Wiebe, R., 1968. Plagioclase stratigraphy; a record of magmatic conditions and events in a granite stock. Am. J. Sci. 266 (8), 690–703. http://dx.doi.org/10.2475/ajs.266.8.690.

Witham, F., 2011. Conduit convection, magma mixing, and melt inclusion trends at persistently degassing volcanoes. Earth Planet. Sci. Lett. 301 (1–2), 345–352. http://dx.doi.org/10.1016/j.epsl.2010.11.017.

Zandomeneghi, D., Aster, R., Kyle, P., Barclay, A., Chaput, J., Knox, H., 2013. Internal structure of Erebus volcano, Antarctica imaged by high-resolution active-source seismic tomography and coda interferometry. J. Geophys. Res., Solid Earth 118 (3), 1067–1078.